Chapter 5

Event Trigger Super Twisting Sliding Mode Control for Microgrid with Matched/Unmatched Disturbance Observer

In this chapter microgrid power system network is considered for control implementation to achieve the thesis objectives of minimized complexity in the control operation of power system networks, to improve the control efforts, compensation of match/mismatch uncertainties in the network, and to enhance robustness of the power system operation. In this chapter of the thesis a novel concept of event-triggering control (ETC) for effective resource utilization is proposed for microgrid. Matched uncertainty elimination is possible through sliding mode control (SMC) itself as addressed in the literature. This chapter of the thesis proposes a new approach for suppression of both matched and unmatched uncertainties in grid-connected and islanded mode through an integral disturbance observer (IDO) which is designed with super twisting SMC to provide dual filtering phenomena pertaining to system perturbations. The IDO facilitates a control algorithm to manage effective event counts during disturbance conditions. The proposed controller is designed in order to regulate DC bus voltage and enhance the microgrid capability to perform stable operations in presence of uncertainties. Chattering free finite time convergent SMC is designed with super twisting reaching law to obtain robust behavior of microgrid. Results are compared with power rate reaching SMC, Nonlinear disturbance observer (NDO) based controller, and PI controller. In the proposed work event triggering condition is designed first time under super twisting reaching law. Comparative assessment is accomplished in lieu of demonstrating the superior performance of event

trigger SMC through MATLAB/Simulink and Typhoon-based controller hardware in loop (CHIL) platform.

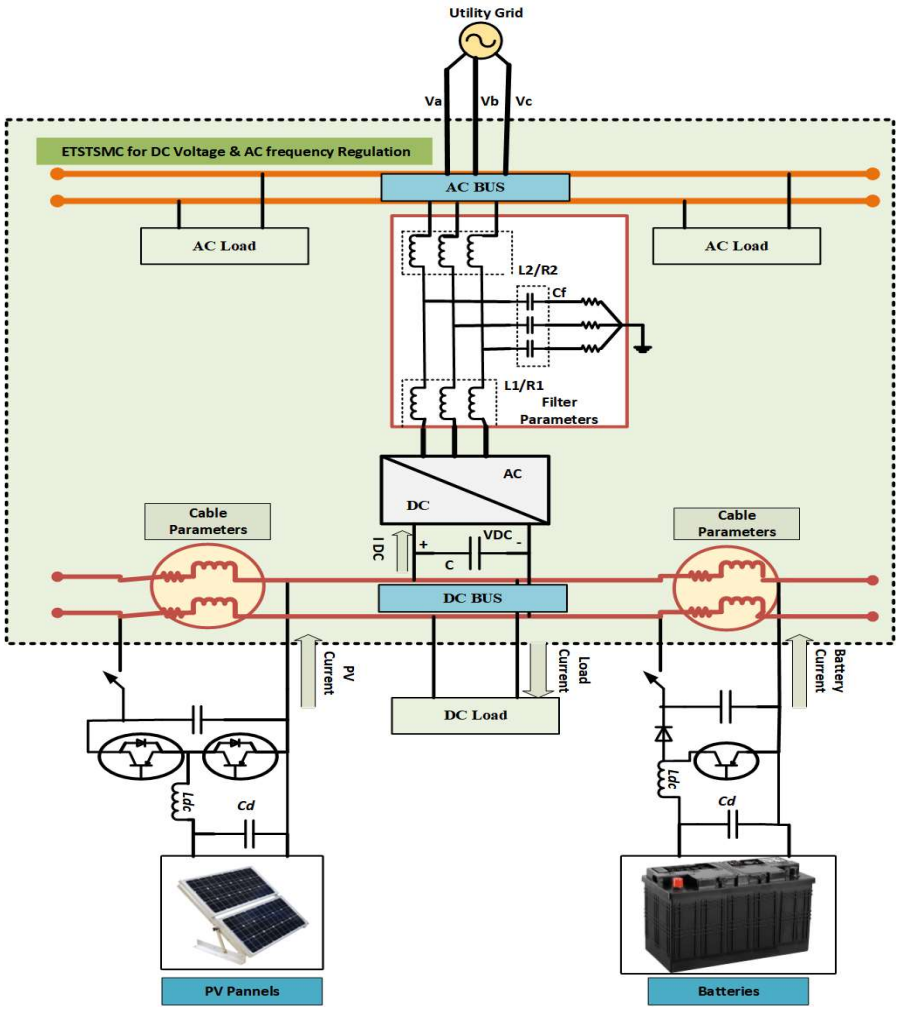

Figure 5.1. Microgrid configuration.

5.1 Introduction

The research in [86]-[88] had explained the dc-ac converter control with respect to dc-bus voltage regulation and power balance monitoring within the microgrid system. Conventional PI based voltage and current control loops in synchronous reference frame are used to ensure dc-bus voltage regulation and current tracking capabilities respectively [89]-[91]. For dc bus voltage regulation further improvement has been introduced in [92]-[95], where the PI control loops are designed to compensate only mismatched disturbances present in the dc system current information. Similarly, in [96], a nonlinear disturbance observer has been designed to compensate dc-bus current disturbance

considered as mismatched information. To achieve adequate control response in these control schemes, communication bandwidth should be enhanced in an appropriate ratio between microgrid assets and inverter system which further affects the microgrid plug-and-play and scalability features. The wide use of robust control has been cited in many current research and has been widely utilized in industrial applications due to its potent ability of disturbance rejection & conceptual modesty [97]-[98]. SMC is one of the eminent robust control techniques which is extensively adopted in power systems nowadays [99]-[102]. In microgrid control aspects the SMC has gained wide publicity as per its efficient and robust performance [103]-[105]. The sliding mode concept applied in microgrid by considering distributed energy storage as a multiagent system is proposed in [103]. In this study SMC based power distribution strategy is used to maintain power sharing between multiagent storage system and its reflection of bus voltage is focused but the effect of other DG's and parametric disturbances on dc bus voltage is not considered. Also, there is no discussion found on time-based triggering for improved resource utilization. Ref. [104] explains SMC based technique for a DC micro-grid in presence of constant power loads. The SMC based control regulates the DC bus voltage under the effect of destabilized power loads. Microgrid scenario is well focused with respect to controller design, but it lacks addressing chattering suppression, matched/unmatched system uncertainties and control effort saving. Similarly [105] also does not include the same features, although adaptive SMC is well proposed to estimate reference power to maintain energy balance among distributed generators (DGs) in hybrid microgrid aspects. In [105], the controller is designed by considering single phase supply. The approach of SMC strategy is implemented in [106] for power sharing in hybrid AC/DC microgrid. A thorough investigation is presented in this chapter of the thesis for tracking reference point, to reject disturbance, enhancing microgrid performance for both small & large-signal disturbances in presence of nonlinear & unbalanced loads, increasing fault tolerant capability and ensuring power sharing to the desired level. It is observed that many of existing sliding surface designs are focused on matched uncertainty mitigation while the sliding motion of conventional SMC is only oblivious to matched uncertainties [107]. The

matched uncertainties are those which occur in the control input channel itself [108]. This matching condition however not be satisfied by many practical systems [109],[110]. To compensate both matched and unmatched uncertainties, a novel IDO is designed along with the sliding mode event-based control triggering in this chapter of the thesis. Therefore, the proposed controller has dual scale filtering for disturbances and uncertainties. This novel approach offers error convergence in finite time, chattering suppression and least resource utilization.

In the recent literatures event-trigger control is featured as one of the eminent approaches [111],[112] as it minimizes the control efforts as well as resource utilization. The technique is based on the desired control events as compared to periodic control implementation. Here the control signal will be updated as per violation of the triggering criteria, so it is a demand-based control technique. Therefore, significant improvement in the system operation can be achieved through event-trigger control law that minimizes control computation effectively. The event trigger sliding mode control (ETSMC) for interconnected microgrid is proposed in [113], where load-frequency control is applied through Adaptive ETSMC but the dc voltage regulation and unmatched uncertainty compensation in microgrid were not evaluated simultaneously. A H_∞ controller robust control scheme in [114] presented an enhanced performance of microgrid under small & large signal disturbance and load unbalance conditions. The proposed scheme improves fault ride through competency through required power-sharing with incorporation to the communication time delay effects [114]. Although numerous works of literature are available in context of design of control schemes but the remarkable effort for the same deteriorates the overall system performance. Thus, an attempt is made to minimize the effort in the control law through event triggering. The advantage of event triggering SMC supplemented by super twisting law is explored in context of DC voltage & AC bus frequency regulation simultaneously. On contrary to mere linearization, the nonlinear control is addressed in the present chapter of the thesis both in matched and unmatched uncertainties. Thus, the noteworthy contribution is highlighted by the following points.

- Voltage regulation in a microgrid is proposed to improve transient and steady-state

performance using super twisting reaching law with finite time convergence simultaneously through IDO design in the microgrid.

- With respect to the proposed controller, threshold criteria for event-triggering super twisting SMC (ETSTSMC) have been derived through Lyapunov theory with the derivation of inter-execution time between consecutive triggering instants.
- Robust control technique under disturbance conditions in a microgrid scenario is proposed with reduced control effort through ETC.
- The main merit of the proposed work is to reduce the event count of the ETSTSMC scheme through the observer in the presence of disturbances.

5.2 Microgrid Model and Problem Identification

A microgrid system is briefly illustrated as in Figure *5.1*. DER sources are shown connected with dc bus and dc load. This micro grid system consists of maximum power point tracking (MPPT) control-based PV arrays followed by boost dc-dc converter stage to maintain appropriate dc level. To compensate variations in PV output, dc load fluctuation, and dispatched demand tracking from central control unit [88], [104], bidirectional energy control is implemented in battery storage system. The inverter unit in between microgrid and utility grid is designed by using 3-Φ pulse width-modulation (PWM) controlled voltage-source inverter (VSI) followed by *LCL* filter section. As mentioned earlier in section-5.2, this interlinking dc-ac converter regulates the dc-bus voltage at desired level and can satisfy the power balance in microgrid system. In this chapter of the thesis the proposed control method of dc-bus voltage regulation is formed as per the system depicted in Figure *5.2*. The respective system is designed using dynamic differential equation for interlink capacitor voltage of microgrid. Dynamical differential equation for the shown capacitor voltage in the microgrid of dc bus can be described by (*5.1*).

$$C\frac{dV_{dc}}{dt} = \left(i_{bat} + i_{pv} - i_{load}\right) - i_{dc} \tag{5.1}$$

Here 'C' denotes dc bus capacitor.V_{dc} , i_{pv}, i_{bat} , i_{load} and i_{dc} represents the dc-bus voltage, output dc currents of the PV unit, battery system, dc load intake and dc current

of the inverter respectively. The inverter in d-q synchronous frame can be modelled (In orientation with grid voltage) as:

$$e_d = L_1\frac{di_{ivd}}{dt} + i_{invd}R_1 + [V_{cd} + (i_{invd} - i_d)R_d] + \omega L_1 i_{invq} \quad 5.2$$

$$e_q = L_1\frac{di_{invq}}{dt} + i_{invq}R_1 + \left[V_{cq} + (i_{invq} - i_q)R_d\right] - \omega L_1 i_{invd} \quad 5.3$$

$$i_{invd} = C_f\frac{dV_{cd}}{dt} + i_d + \omega C_f V_{cq} \quad 5.4$$

$$i_{invq} = C_f\frac{dV_{cq}}{dt} + i_q - \omega C_f V_{cd} \quad 5.5$$

$$V_{cd} + (i_{invd} - i_d)R_d = L_2\frac{di_d}{dt} + i_d R_2 + U_d + \omega L_2 i_q \quad 5.6$$

$$V_{cq} + \left(i_{invq} - i_q\right)R_d = L_2\frac{di_q}{dt} + i_q R_2 - \omega L_2 i_d \quad 5.7$$

The e_d and e_q represents direct & quadrature components of dc-ac converter output voltage. U_d and U_q are direct and quadrature component of grid voltage. The quadrature component U_q is taken zero as dq frame is oriented with grid voltage. i_d and i_q are respective active, reactive components of grid current. ω is the fundamental angular frequency. L_1 and L_2 represents the inductances of filter depicted in Figure *5.1*. R_1 and R_2 are describing the parasitic resistances of the filter inductances and system loss; C_f is the filter capacitance and R_d is denoting the damping resistance. i_{invd} & i_{invq} are the active-reactive components of the converter side currents respectively. The notation V_{cd} and V_{cq} are direct and quadrature axis components of filter capacitance voltage. The effect of filter capacitance (mainly considered for low frequency range) [115],[116] can be neglected for the controller design as high frequency current ripples are mitigated through LCL filter. The closed loop control is to be designed with bandwidth less than the LCL filter's resonant frequency [91].

Consequently, the inverter output voltage, grid voltage and grid side current can be synthesized in dq frame [96] as.

$$e_d = U_d + L\frac{di_d}{dt} + \omega L i_q + i_d R \quad 5.8$$

$$e_q = L\frac{di_q}{dt} - \omega L i_d + i_q R \tag{5.9}$$

Here $L = (L_1 + L_2)\ and\ \ R = (R_1 + R_2)$

Now, if the conversion loss of the inverter is neglected, active power sharing between DC bus and AC bus can be derived as:

$$P_g = V_{dc} i_d = \frac{3}{2} U_d i_d \tag{5.10}$$

Expression shown in (*5.11*) will represent the second-order DC bus voltage control which is derived by rearranging (*5.1*), (*5.8*), (*5.9*) and (*5.10*).

$$\left.\begin{aligned} \frac{dV_{dc}}{dt} &= -\frac{3U_d i_d}{2CV_{dc}} + \frac{i_o}{C} \\ \frac{di_d}{dt} &= -\frac{R}{L} i_d - \omega i_q + \frac{e_d - U_d}{L} \\ \frac{di_q}{dt} &= -\frac{R}{L} i_q - \omega i_d + \frac{e_q}{L} \end{aligned}\right\} \tag{5.11}$$

where $i_o = (i_{batt} + i_{pv} - i_{load})$.

5.3 Sliding Mode Controller Designing with Super Twisting reaching Law for Microgrid

Equation (*5.11*) can be expressed in a generalized form as (*5.12*).

$$\dot{x} = f(x) + (\mathcal{J})U \tag{5.12}$$

$f(x)$ is the nonlinear function of the system states that is given as:

$$f(x) = \begin{bmatrix} -\frac{3U_d i_d}{2CV_{dc}} + \frac{i_o}{C} \\ -\frac{R}{L} i_d - \omega i_q - \frac{U_d}{L} \\ -\frac{R}{L} i_q - \omega i_d \end{bmatrix} \text{ and } \mathcal{J} = \begin{bmatrix} 0 & 0 \\ 1/L & 0 \\ 0 & 1/L \end{bmatrix}.$$

The control inputs for the system are considered as the inverter output voltage components. Sliding mode control is designed in a way to achieve desired references within a finite time. The error dynamic states for the microgrid system as per (*5.11*) can be designed as:

$$\left.\begin{aligned} V_{dce} &= V_{dc} - V_{dcref} \\ i_{de} &= i_d - i_{dref} \\ i_{qe} &= i_q - i_{qref} \end{aligned}\right\} \tag{5.13}$$

The error dynamic model can be designed from (*5.12*) and (*5.13*) described as:

$$\dot{x}_e = f(x_e) + (\mathcal{J})U \tag{5.14}$$

Where $x_e = x - x_{ref}$ as given in (*5.13*). The x_{ref} represent the reference or desired state value. Here V_{dcref} is assumed to be constant. The values of i_{dref} and i_{qref} are slow changing variables that can be approximated as constant. Therefor the error dynamics of system can be expressed as $\dot{x}_e = f(x) + (\mathcal{J})U$. Sliding surface is now designed in a way to track the desired trajectory. Super twisting sliding surface is designed for significant chattering suppression. Here each error state is taken as the individual sliding surface. $S_1 = x_e$ and $\dot{S}_1 = \dot{x_e}$ therefor,

$$\dot{S}_1 = f(x_e) + (\mathcal{J})U \tag{5.15}$$

The control input for the system is then can be represented as:

$$U = \mathcal{J}^{-1}[-f(x_e) + \dot{S}_1] \tag{5.16}$$

$$\dot{S}_1 = -\lambda_{min}(K_1)|S_1|^{\frac{1}{2}} sign(S_1) + S_2 = -\lambda_{min}(K_1)\frac{S_1}{\|S_1\|^{\frac{1}{2}}} + S_2 \tag{5.17}$$

$$\dot{S}_2 = -\lambda_{min}(K_2) sign(S_1) = -\lambda_{min}(K_2)\frac{S_1}{\|S_1\|} \tag{5.18}$$

Where $k_i \; for \; (i = 1,2)$ is a square positive definite diagonal matrix having all positive elements $(k_i > 0, k_i \in R^{+}_{3\times3})$ provided in Table 5.1. $S_i \; for \; (i = 1,2)$ denotes the sliding surface vector. The variable $\mathcal{J}$ used in (5.15), is a non-square matrix, thus can be evaluated by pseudo inverse method. Super twisting has an advantage over power rate reaching law that it is more robust against disturbances with simultaneous chattering elimination. Power rate reaching law SMC (PRSMC) can be expressed as [118], $\dot{S} = -\lambda_{min}(K_{pr})|S|^{\partial} sgn(S)$ where $\lambda_{min}(K_{pr}) > 0$ & $0 < \partial < 1$.

5.3.1. Proposed Event Trigger Approach Under Super Twisting SMC Law

Event trigger condition can be derived as per the following analysis. The triggering rule is designed in such a way that control signal will update only when system error states violate the predefined threshold. On the other hand, if error states are following the defined constrain then previous control input will retain. In this way the control input will remain constant between two inter execution times t & t_i and can be expressed as:

$$U(t) = \mathcal{J}^{-1}[-f(x_e(t_i)) + \dot{S}_1(t_i)] \quad 5.19$$

For the instance $t \in [t, t_i]$.

5.3.2. Condition for event-based trigger control

An event trigger error can be expressed as $x_e = x(t_i) - x(t)$ such that $x_e = 0$ at $t = t_i$. If the magnitude of state error x_e violates the threshold condition, then the updated control will be executed otherwise previously updated control will retain.

Assumption 1 A non-linear functions used as $f(x_e)$ is assumed to be locally lipschitz for a lipschitz constant ($\mathcal{L}$) in such a way that $\|f(x_e)\| = \mathcal{L}\|x_e\|$

Here $\|.\|$, represents the second norm of the respective function (.).

Assumption 2 For determining event-trigger condition for the system represented in (*5.12*), this is assumed that functions $f(x_e)$ is Lipschitz to its argument in a way that:

$$\|f(x_e(t)) - \mathfrak{Z} f(x_e(t_i))\| < \mathcal{L}_1 \|x \ (t) - x_e(t_i)\| = \mathcal{L}_1\|x_{e\Delta}\|$$

Theorem 1: If following evet-triggering condition is violated with respect to error states then the controller will update its input as per (*5.16*).

$$\|x_{e\Delta}\| < \frac{\mathfrak{Z}\lambda_{min}(K_1)\|S_1\|^{\frac{1}{2}} - \mathfrak{Z}\mathcal{L}_a\|S_1\|}{\mathcal{L}_1} \quad 5.20$$

Proof 1: In the SMC technique, Lyapunov stability criterion is applied for operating conditions of the control logic, which will follow the zero equilibrium states trajectory. A strictly positive Lyapunov function (V) is selected as:

$$V = \left(\frac{2K_2 + 1}{K_1}\right)\|S_1\| + \frac{2S_2^T S_1}{\|S_1\|^{1/2}} + \left(\frac{1 + K_1^2 + 2K_2}{K_1 K_2}\right)S_2^T S_2$$

The strict positiveness of the Lyapunov function is proven in [117]. The K_1, K_2 is to be represented in their minimum eigen values as $\lambda_{min}(K_1)$ & $\lambda_{min}(K_2)$ respectively.

$$V \leq \left(\frac{2\lambda_{min}(K_2) + 1}{\lambda_{min}(K_1)}\right)\|S_1\| + \frac{2S_2^T S_1}{\|S_1\|^{1/2}} + \left(\frac{1 + [\lambda_{min}(K_1)]^2 + 2\lambda_{min}(K_2)}{\lambda_{min}(K_1)\,\lambda_{min}(K_2)}\right)S_2^T S_2 \quad 5.21$$

A finite time converge of sliding surfaces must follow the lemma expressed as,

Lemma 1: For any continuous time, system $\dot{đ} = ƒ(đ)$, where $ƒ(0) = 0$ and $đ \in \mathbb{R}^m$, A positive definite continuous Lyapunov function is assumed as $V: \mathbb{R}^m \rightarrow \mathbb{R}$, with open neighborhood of $U \subset \mathbb{R}^m$ of any surface ($đ$) so as the following inequality given in (*5.21*)

satisfies.

$$\dot{V}(đ) \leq 0, đ \in U \tag{5.22}$$

Then the converge of sliding surface to stable equilibrium point is ensured [120]. Form (*5.22*) the derivative of Lyapunov function ($\dot{V}$) can be written as:

$$\dot{V} \leq \left(\frac{2\lambda_{min}(K_2) + 1}{\lambda_{min}(K_1)}\right)\frac{S_1^T\dot{S}_1}{\|S_1\|} + \frac{2S_2^T\dot{S}_1}{\|S_1\|^{1/2}} + \frac{2\dot{S}_2{}^T S_1}{\|S_1\|^{1/2}} + \left(\frac{1 + [\lambda_{min}(K_1)]^2 + 2\lambda_{min}(K_2)}{\lambda_{min}(K_1)\,\lambda_{min}(K_2)}\right)S_2^T\dot{S}_2 \tag{5.23}$$

From (*5.15*),

$$\dot{S}_1(t_i) = f(x_e(t_i)) + (\mathcal{J})U(t_i) \tag{5.24}$$

From (*5.23*) and (*5.24*)

$$\dot{V} \leq \left(\frac{2\lambda_{min}(K_2)+1}{\lambda_{min}(K_1)}\right)\left\{\frac{S_1^T[f(x_e(t_i))+(\mathcal{J})U(t_i)]}{\|S_1\|}\right\} + \frac{2S_2^T[f(x_e(t_i))+(\mathcal{J})U(t_i)]}{\|S_1\|^{1/2}} + \frac{2\dot{S}_2{}^T S_1}{\|S_1\|^{1/2}} + \left(\frac{1+[\lambda_{min}(K_1)]^2+2\lambda_{min}(K_2)}{\lambda_{min}(K_1)\,\lambda_{min}(K_2)}\right)S_2^T\dot{S}_2$$

Placing value of $U(t_i)$ from (*5.9*) in above equation

$$\dot{V} \leq \left(\frac{2\lambda_{min}(K_2)+1}{\lambda_{min}(K_1)}\right)\left\{\frac{S_1^T[f(x_e(t_i))+\mathcal{J}\mathcal{J}^{-1}[-f(x_e(t_i))+\dot{S}_1(t_i)]]}{\|S_1\|}\right\} + \frac{2S_2^T[f(x_e(t_i))+\mathcal{J}\mathcal{J}^{-1}[-f(x_e(t_i))+\dot{S}_1(t_i)]]}{\|S_1\|^{1/2}} + \frac{2\dot{S}_2{}^T S_1}{\|S_1\|^{1/2}} + \left(\frac{1+[\lambda_{min}(K_1)]^2+2\lambda_{min}(K_2)}{\lambda_{min}(K_1)\lambda_{min}(K_2)}\right)S_2^T\dot{S}_2$$

Now by putting $\dot{S}_1$ and $\dot{S}_2$ from (*5.17*) and (*5.18*) in above equation.

$$\dot{V} \leq \left(\frac{2\lambda_{min}(K_2)+1}{\lambda_{min}(K_1)}\right)\left\{\frac{S_1^T[f(x_e(t_i))-\mathfrak{F}f(x_e(t_i))-\lambda_{min}(K_1)\mathfrak{F}\frac{S_1(t_i)}{\|S_1\|^{\frac{1}{2}}}+\mathfrak{F}S_2(t_i)]}{\|S_1\|}\right\} + \frac{2S_2^T\left[f(x_e(t_i))-\mathfrak{F}f(x_e(t_i))-\lambda_{min}(K_1)\mathfrak{F}\frac{S_1(t_i)}{\|S_1\|^{\frac{1}{2}}}+\mathfrak{F}S_2(t_i)\right]}{\|S_1\|^{1/2}} - \frac{2\lambda_{min}(K_2)S_1{}^T S_1}{\|S_1\|\|S_1\|^{1/2}} - \left(\frac{1+[\lambda_{min}(K_1)]^2+2\lambda_{min}(K_2)}{\lambda_{min}(K_1)}\right)S_2^T\frac{S_1}{\|S_1\|}$$

Where $\mathfrak{F} = \mathcal{J}\mathcal{J}^{-1}$

Since $S_2 = -\lambda_{min}(K_2)\int_0^t sign(S_1)$ so under Lipschitz condition $\|S_2\| = \mathcal{L}_a\|S_1\|$. And using lemma 1.

$$\dot{V} \leq \left(\frac{2\lambda_{min}(K_2)+1}{\lambda_{min}(K_1)}\right)\left\{\frac{\mathcal{L}_1\|x_{e\Delta}\|\|S_1\|-\mathfrak{F}\lambda_{min}(K_1)\frac{S_1^T S_1(t_i)}{\|S_1\|^{\frac{1}{2}}}+\mathfrak{F}S_1^T S_2(t_i)}{\|S_1\|}\right\}+$$

$$\frac{2\left[\mathcal{L}_1\|x_{e\Delta}\|\|S_2\|-\mathfrak{F}\lambda_{min}(K_1)\frac{S_2^T S_1(t_i)}{\|S_1\|^{\frac{1}{2}}}+\mathfrak{F}S_2^T S_2(t_i)\right]}{\|S_1\|^{1/2}} - 2\lambda_{min}(K_2)\|S_1\|^{1/2} -$$

$$\left(\frac{1+[\lambda_{min}(K_1)]^2+2\lambda_{min}(K_2)}{\lambda_{min}(K_1)}\right)S_2^T\|S_1\|$$

The above equation can be further modified as

$$\dot{V} \leq \left(\frac{2\lambda_{min}(K_2)+1}{\lambda_{min}(K_1)}\right)\left\{\mathcal{L}_1\|x_{e\Delta}\| - \mathfrak{F}\lambda_{min}(K_1)\|S_1\|^{\frac{1}{2}} + \mathfrak{F}\mathcal{L}_a\|S_1\|\right\} + 2\|S_1\|^{\frac{1}{2}}\left\{\mathcal{L}_1\mathcal{L}_a\|x_{e\Delta}\| -\right.$$

$$\left.\mathfrak{F}\mathcal{L}_a\lambda_{min}(K_1)\|S_1\|^{1/2} + \mathfrak{F}\mathcal{L}_a\|S_1\|\right\} - 2\lambda_{min}(K_2)\|S_1\|^{\frac{1}{2}} -$$

$$\left(\frac{1+[\lambda_{min}(K_1)]^2+2\lambda_{min}(K_2)}{\lambda_{min}(K_1)}\right)\mathcal{L}_a\|S_1\|^2$$

From the above equation the event triggering conditions to make Lyapunov derivative function strictly negative is obtained as provided in (*5.20*).

5.3.3. Proof of the Stability and Robustness

For stability of the microgrid against SMC sliding surfaces, it is desirable to have $\frac{dV}{dt} < 0$.

The stability of the system is ensured as per the following proof.

In (*5.23*), substituting values of $\dot{S}_1$ *and* $\dot{S}_2$ from (*5.17*), (*5.18*).

$$\dot{V} \leq \left(\frac{2\lambda_{min}(K_2)+1}{\lambda_{min}(K_1)}\right)\frac{S_1^T}{\|S_1\|}\left[-\lambda_{min}(K_1)\frac{S_1}{\|S_1\|^{1/2}} + S_2\right] + \frac{2S_2^T}{\|S_1\|^{1/2}}\left[-\lambda_{min}(K_1)\frac{S_1}{\|S_1\|^{1/2}} + S_2\right] +$$

$$\frac{2S_1}{\|S_1\|^{1/2}}\left[-\lambda_{min}(K_2)\frac{S_1}{\|S_1\|}\right]^T + \left(\frac{1+[\lambda_{min}(K_1)]^2+2\lambda_{min}(K_2)}{\lambda_{min}(K_1)\,\lambda_{min}(K_2)}\right)S_2^T\left[-\lambda_{min}(K_2)\frac{S_1}{\|S_1\|}\right]$$

or

$$\dot{V} \leq -(2\lambda_{min}(K_2)\ +1)\frac{S_1^T S_1}{\|S_1\|^{3/2}} + \left(\frac{2\lambda_{min}(K_2)+1}{\lambda_{min}(K_1)}\right)\frac{S_1^T S_2}{\|S_1\|} - \frac{2\lambda_{min}(K_1)S_2^T S_1}{\|S_1\|} + \frac{2S_2^T S_2}{\|S_1\|^{1/2}} -$$

$$\frac{2\lambda_{min}(K_2)S_1^T S_1}{\|S_1\|^{3/2}} - \left(\frac{1+[\lambda_{min}(K_1)]^2+2\lambda_{min}(K_2)}{\lambda_{min}(K_1)\,\lambda_{min}(K_2)}\right)\left[\frac{S_2^T S_1}{\|S_1\|}\right]$$

or

$$\dot{V} \leq -(2\lambda_{min}(K_2)\ +1)\frac{S_1^T S_1}{\|S_1\|^{3/2}} - 2\lambda_{min}(K_2)\frac{S_1^T S_1}{\|S_1\|^{3/2}} + \left[-\frac{3\lambda_{min}(K_1)S_2^T S_1}{\|S_1\|} + \frac{2S_2^T S_2}{\|S_1\|^{1/2}}\right]$$

or

$$\dot{V} < -(2\lambda_{min}(K_2) + 1)\|S_1\|^{1/2} - 2\lambda_{min}(K_2)\|S_1\|^{1/2} + \left[-3\lambda_{min}(K_1)\|S_2\| + \frac{2\|S_2\|^2}{\|S_1\|^{1/2}}\right]$$

$$= -(2\lambda_{min}(K_2) + 1)\|S_1\|^{1/2} - 2\lambda_{min}(K_2)\|S_1\|^{1/2} - \|S_2\|\left[3\lambda_{min}(K_1) - \frac{2\|S_2\|}{\|S_1\|^{1/2}}\right]$$

From this, the condition for stability can be achieved as

$$\frac{3}{2}\lambda_{min}(K_1)\|S_1\|^{1/2} > \|S_2\|$$

Using Lipschitz inequality ($\|S_2\| = \mathcal{L}_a\|S_1\|$), under condition $\lambda_{min}(K_1) > \frac{2\mathcal{L}_a}{3}\|S_1\|^{1/2}$, (*5.23*) will be negative definite.

5.3.4. Calculation of inter execution time for finite time convergence.

The inter execution time can be defined by the difference of two consecutive execution time instance as ($T_{ie} = t - t_i$). In this time interval the system states event-triggering error $\|x_{e\Delta}\|$ reaches to $\frac{\eth\lambda_{min}(K_1)\|S_1\|^{\frac{1}{2}} - \eth\mathcal{L}_a\|S_1\|}{\mathcal{L}_1}$ from zero. For evaluating the expression for execution time interval named as inter execution time assumptions 1 and 2 are considered in the respective proof of theorem 2.

Theorem 2: System (*5.14*) representing the microgrid system is controlled as per law (*5.16*) which is updated at i^{th} interval of time with event-trigger condition designed in (*5.20*), then the lower bound for inter execution time T_{ie} by a positive value can be expressed as in (*5.25*):

$$T_{ie} \geq \frac{1}{\mathcal{L}_{a_1}} ln\left(1 + \frac{\mathcal{L}_{a_1}\left[\eth\lambda_{min}(K_1)\|S_1\|^{\frac{1}{2}} - \eth\mathcal{L}_a\|S_1\|\right]}{\mathcal{L}_1\mathcal{L}_A\|x_e(t)\|}\right) \tag{5.25}$$

Proof 2: Inter execution time can be evaluated by differentiating the error states in order to achieve state error variation per unit time.

$$\frac{d\|x_{e\Delta}\|}{dt} \leq \left\|\frac{dx_e}{dt} - \frac{dx_e(t_i)}{dt}\right\|$$

$$= \left\|\frac{d}{dt}\left(x_e(t_i)\right)\right\| = \left\|f(x_e) + (\mathcal{J})U_{eq}(t_i)\right\|$$

$$= \left\|f(x_e) + \mathcal{J}\mathcal{J}^{-1}\left[-f\left(x_e(t_i)\right) - \lambda_{min}(K_1)\frac{S_1(t_i)}{\|S_1\|^{\frac{1}{2}}} + S_2(t_i)\right]\right\|$$

$$= \left\| f(x_e) - \mathfrak{Z} f\left(x_e(t_i)\right) - \mathfrak{Z}\lambda_{min}(K_1)\frac{S_1(t_i)}{\|S_1\|^{\frac{1}{2}}} + \mathfrak{Z}S_2(t_i) \right\|$$

$$= \mathcal{L}_{a_1}\|x_e(t)\| + \mathfrak{Z}\mathcal{L}_{a_2}\|x_e(t_i)\| + \mathfrak{Z}\lambda_{min}(K_1)\mathcal{L}_{a_3}\|x_e(t)\| + \mathfrak{Z}\mathcal{L}_{a_4}\|x_e(t)\|$$

$$= \mathcal{L}_{a_1}\|x_{e\Delta} + x_e(t_i)\| + \mathfrak{Z}\mathcal{L}_{a_2}\|x_e(t_i)\| + \mathfrak{Z}\lambda_{min}(K_1)\mathcal{L}_{a_3}\|x_e(t)\| + \mathfrak{Z}\mathcal{L}_{a_4}\|x_e(t)\|$$

$$= \mathcal{L}_{a_1}\|x_{e\Delta}\| + \mathcal{L}_{a_1}\|x_e(t_i)\| + \mathfrak{Z}\mathcal{L}_{a_2}\|x_e(t_i)\| + \mathfrak{Z}\lambda_{min}(K_1)\mathcal{L}_{a_3}\|x_e(t)\| + \mathfrak{Z}\mathcal{L}_{a_4}\|x_e(t)\|$$

$$\frac{d\|x_{e\Delta}\|}{dt} - \mathcal{L}_{a_1}\|x_{e\Delta}\| = [\mathcal{L}_{a_1} + \mathfrak{Z}\mathcal{L}_{a_2} + \mathfrak{Z}\lambda_{min}(K_1)\mathcal{L}_{a_3} + \mathfrak{Z}\mathcal{L}_{a_4}]\ \|x_e(t)\| \quad 5.26$$

By putting $\mathcal{L}_A = \mathcal{L}_{a_1} + \mathfrak{Z}\mathcal{L}_{a_2} + \mathfrak{Z}\lambda_{min}(K_1)\mathcal{L}_{a_3} + \mathfrak{Z}\mathcal{L}_{a_4}$ in (*5.26*).

$$\frac{d\|x_{e\Delta}\|}{dt} - \mathcal{L}_{a_1}\|x_{e\Delta}\| = \mathcal{L}_A\ \|x_e(t)\| \quad 5.27$$

For $t \in [t, t_i]$, the solution of the differential inequality (*5.27*) is obtained by summoning the comparison Lemma-3.4 stated in [Khalil, 2002] with initial condition $\|x_e(t_i)\|= 0$ as:

$$\|x_{e\Delta}\| \leq \frac{\mathcal{L}_A\|x_e(t)\|\left(exp^{\mathcal{L}_{a_1}(t-t_i)} - 1\right)}{\mathcal{L}_{a_1}} \quad 5.28$$

Next triggering instant t_i will satisfy triggering rule (*5.20*) and at this instant (*5.28*) will follow the inequality,

$$\frac{\mathfrak{Z}\lambda_{min}(K_1)\|S_1\|^{\frac{1}{2}} - \mathfrak{Z}\mathcal{L}_a\|S_1\|}{\mathcal{L}_1} \leq \frac{\mathcal{L}_A\|x_e(t)\|\left(exp^{\mathcal{L}_{a_1}(t-t_i)} - 1\right)}{\mathcal{L}_{a_1}} \quad 5.29$$

Rearrangement of (*5.29*) provides the expression for inter execution time presented in (*5.25*). The expression for T_{ie} shows that the inequality is lower bounded by a fixed positive value as $\mathcal{L}_A\|x_e(t)\|$ for $\|x(t_i)\| \neq 0$. Hence the microgrid system will be asymptotically stable. It is also observed that T_{ie} will always be bounded by a fixed positive value.

5.4 Sliding Mode Based IDO Design

5.4.1. Matched/Unmatched uncertainty formulation.

The matched and unmatched uncertainty can be formulated as:

$$\emptyset(e) = \emptyset_m(e) + \emptyset_{um}(e) \quad 5.30$$

Where $\emptyset_m(e)$ and $\emptyset_{um}(e)$ represents matched and unmatched uncertainties respectively. These can mathematically be presented as $\emptyset_m(e) = \mathcal{II}^{\aleph}\emptyset(e)$ and $\emptyset_{um}(e) = \mathcal{I}^{\intercal}(\mathcal{I}^{\intercal})^{\aleph}\emptyset(e)$

Where $g^{\aleph} = [g^T g]^{-1} g^T$.

And $\mathcal{J}^{\urcorner}$ is calculated by solving the inequality, $\mathcal{J}^{\urcorner T} \mathcal{J} = [0 \quad 0]$

$\mathcal{J}^{\urcorner}$ is find as $\mathcal{J}^{\urcorner} = \begin{bmatrix} 1 \\ 0 \\ 0 \end{bmatrix}$.

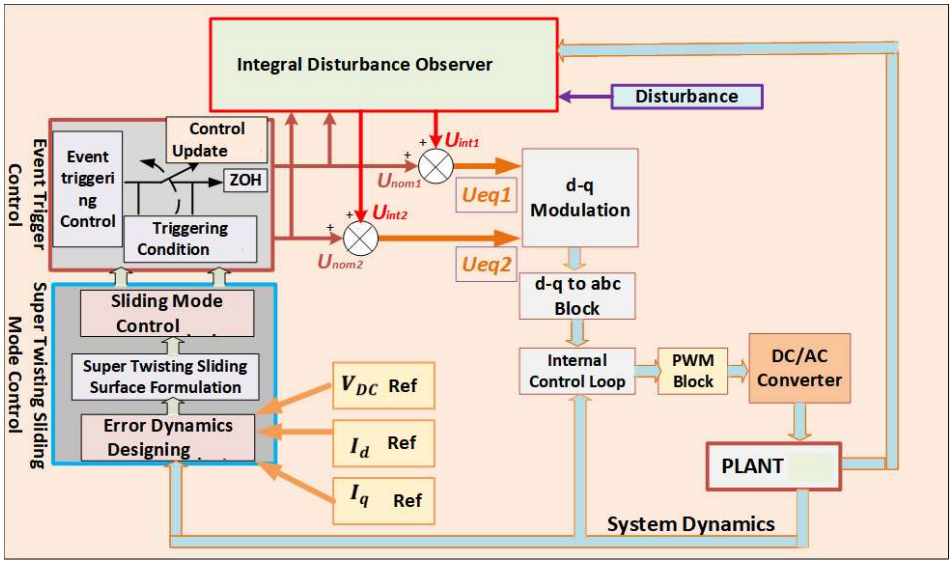

Figure 5.2. Proposed ETSTSMC technique for microgrid.

SYSTEM PROPERTIES AND SPECIFICATIONS

Subsystem	Quantity	Specification
Bidirectional Converter	Grid Voltage	400 V
	Filter capacitance	50 μF
	Parasitic Resistances	$R_1 = 0.04\Omega, R_2 = 0.01\Omega$
	Damping resistance	$R_f = 1.5\Omega$
	Switch frequency	3kHz
	Filter Inductance	$L_1 = 4mH, L_2 = 1mH$
	ω/v ratio	m=0.084
DC Bus	Bus Capacitance	$C = 0.25$F
	Bus Voltage reference	600 V
	Load (DC)	250Ω
DER Parameters	Storage System	200 Ah
	Photovoltaic Power	$5kW$
	DC-DC Converter	$L_{dc} = 5mH, f_{dc} = 3kHz$
AC Load	Star connected Three Phase RL Load	R = 180 $m\Omega$, L = 220 μH
SMC control Parameters	Sliding gain coefficients	$k_1 = 1.43, k_2 = 2.21, k_3 = 1.12, k_4 = 4.18$ $K_d = 3.11$
	Lipschitz constant and Projection coefficient	$\mathcal{L}_1 = 0.21$, $\mathcal{L}_{a_1} = 0.11, \mathcal{L}_{a_2} = 1.01$, $\mathcal{L}_{a_3} = 0.97, \mathcal{L}_{a_4} = 1.21$, $\mathfrak{z} = 0.32$

Table 5.1. System Properties and Specifications

5.4.2. IDO Design for Matched/Unmatched uncertainty

In order to eliminate matched/unmatched uncertainties a sliding surface S_{dis} is designed as in (*5.31*). In (*5.31*) G is representing projection matrix, it is designed so that, $[\mathrm{G}(\mathcal{J})]^{-1}$ exist and will be nonsingular [28]. The designed surface includes system state parameters and an integral term for exponential decay of the disturbances intruded in the system.

$$S_{dis} = \mathrm{G}[x(t) - x(t_0) - \int_0^t (f(x) + (\mathcal{J})U_{nom})dt\,] \tag{5.31}$$

Here G is defined as $\mathcal{J}^T$. U_{nom} is the nominal control output of ETSMC. $x(t_0)$ denotes the values of system states at the initial instant (t_0). Now taking the derivative of (*5.31*).

$$\dot{S}_{dis} = \mathrm{G}[\dot{x}(t) - f(x) - (\mathcal{J})U_{nom}] \tag{5.32}$$

By placing system dynamics in (*5.32*),

$$\dot{S}_{dis} = \mathrm{G}[\{f(x) + (\mathcal{J})U + \emptyset(e)\} - f(x) - (\mathcal{J})U_{nom}] \tag{5.33}$$

Here U is the plant control input. $\emptyset(e)$ is the intruded matched/unmatched disturbance in the system. Here the plant control input is determined by (*5.34*).

$$U = U_{nom} + U_{int} \tag{5.34}$$

From (*5.33*) and (*5.34*), the (*5.35*) is obtained as:

$$\dot{S}_{dis} = \mathrm{G}[f(x) + (\mathcal{J})\{U_{nom} + U_{int}\} + \mathcal{J}\mathcal{J}^{\aleph}\emptyset(e) + \mathcal{J}^{\urcorner}(\mathcal{J}^{\urcorner})^{\aleph}\emptyset(e) - f(x) - (\mathcal{J})U_{nom}] \tag{5.35}$$

By solving (*5.35*), integral control input for disturbance compensation is obtained as:

$$U_{int} = (\mathrm{G}\mathcal{J})^{-1}\left[-\mathrm{G}\emptyset_{um}(e) + \dot{S}_{int}\right] - \mathcal{J}^{\aleph}\emptyset(e) \tag{5.36}$$

Where $\dot{S}_{int} = -\lambda_{min}(K_3)|S_{int}|^{\frac{1}{2}}sign(S_{int}) + \beta_{int}$ and $\dot{\beta}_{int} = -\lambda_{min}(K_4)sign(S_{int})$. As per Figure *5.2* the two equivalent plant controllers are designed from the robust sliding mode control (U_{nom}) and with the IDO (U_{int}) to eliminate both matched and unmatched uncertainties. The error dynamics for proposed ETSTSMC is designed using reference values calculated by matching the power ratings of each DG with the grid. The stability of whole system is achieved in both grid connected and islanded mode by the internal control loop and continuous feedback depicted in Figure *5.2*. Both the proposed ETSTSMC controller and IDO work in cooperation by continuously accessing the output states of AC side as per closed loop feedback system to generate equivalent control output. Internal

control block compares the reference signal from the controller and the output feedback that generates signal for PWM of the converter and maintain system stability. The novel event trigger approach is added with SMC technique in order to minimize resource utilization. All control technique applied on microgrid in this chapter of the thesis is explained through the flowchart shown in Figure 5.3.

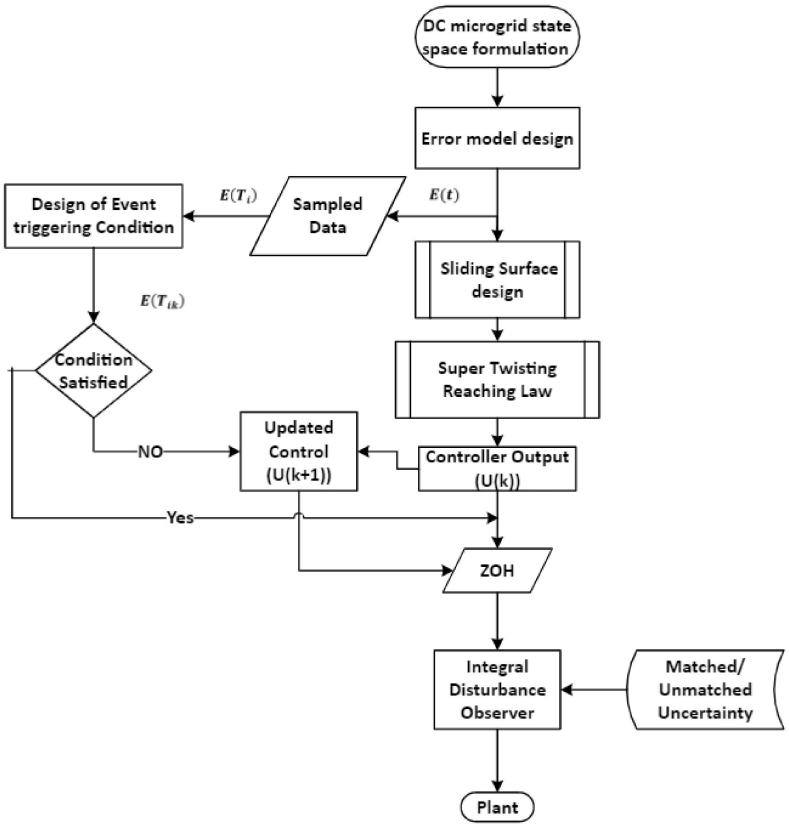

Figure 5.3. Flowchart of proposed ETSTSMC technique for microgrid.

5.5 Result Verification of Microgrid Control

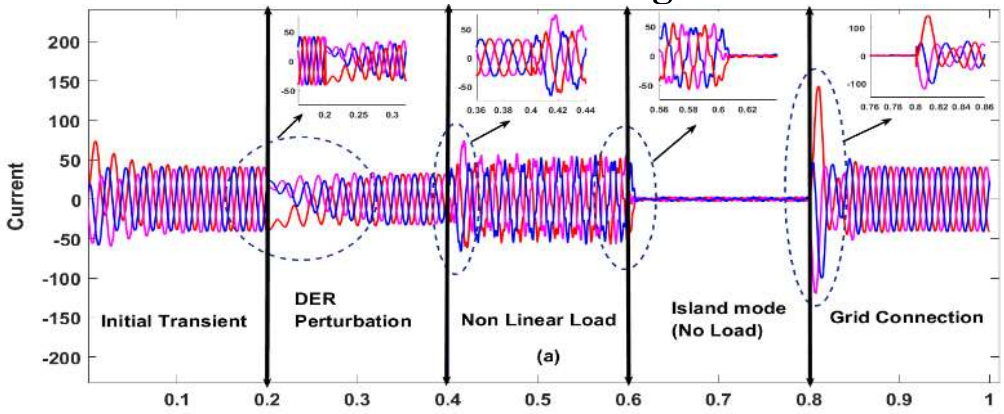

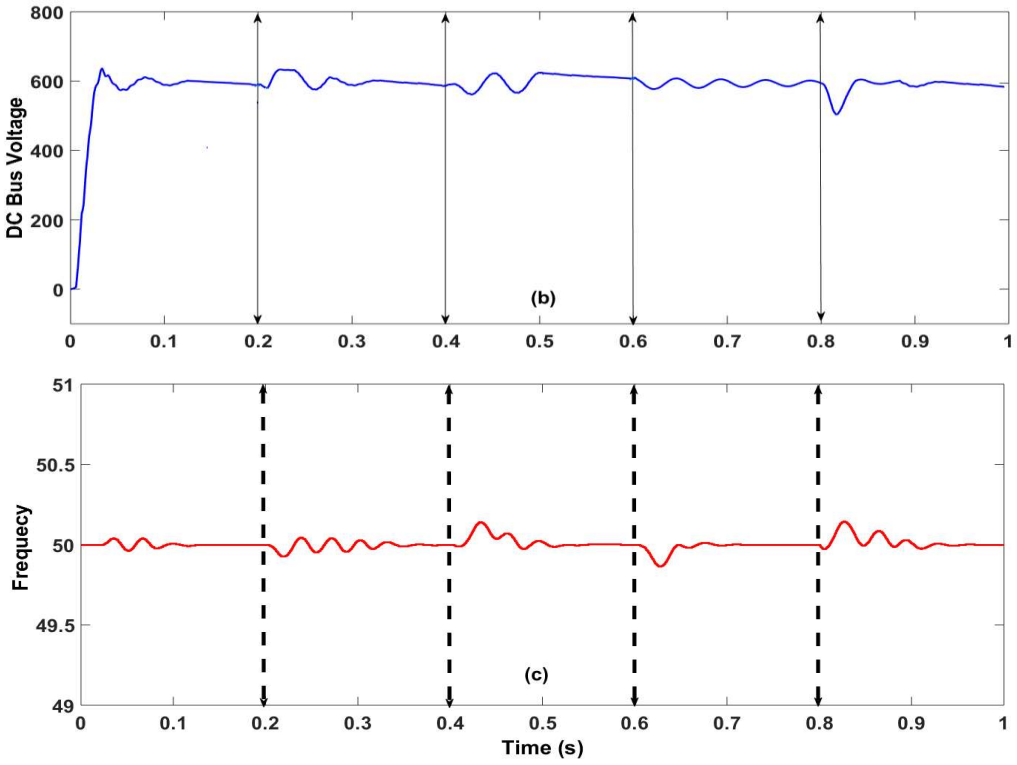

Figure 5.4. Response of signals under disturbances (a) Current Response (b) DC voltage (c) inverter frequency

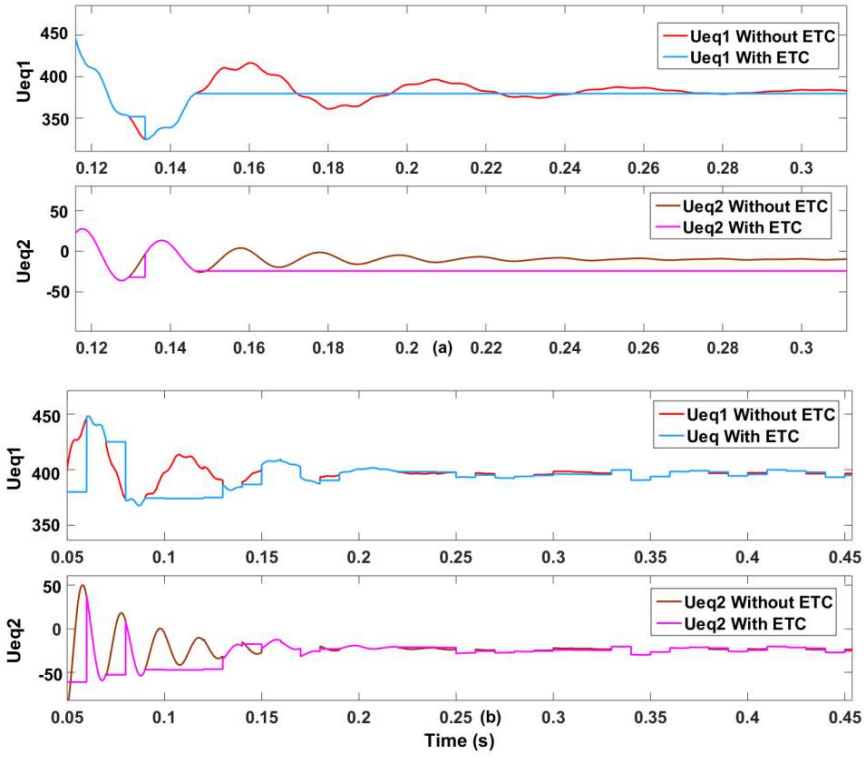

Figure 5.5. Controller Response (a) without noise (b) with noise addition.

The proposed control scheme is verified using MATLAB/Simulink software and with Typhoon based real time simulator. For the verification in both environment 20 kVA rating dc-ac converter system is used. Table *5.1* specifies all the parameters used in the system which is modelled as per Figure *5.1*. Microgrid state deviation under disturbance condition is verified under various perturbations explained in Figure *5.4*. Different perturbations are introduced by disconnecting one of the distributed energy resources (DER), adding nonlinear loads at ac side, introducing island mode at no load condition, and applying grid connection mode respectively.

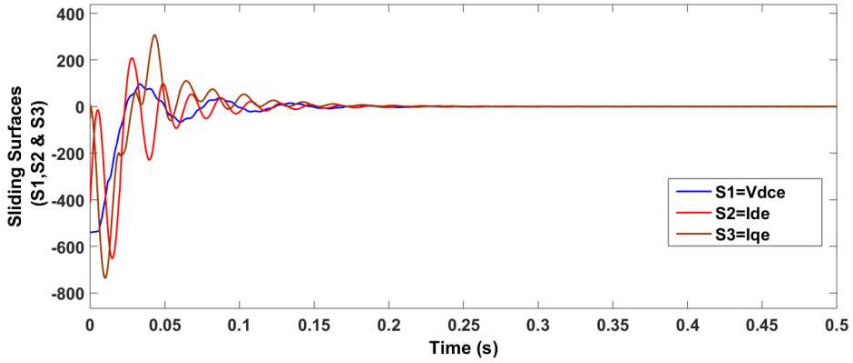

Figure 5.6. Sliding Surface response.

Here the nonlinear load is used as 3-Φ diode rectifier with reverse connection having DC side as series RL Load. Figure *5.4*(a) represents the dc-ac converter current under these perturbations applied for 0.2s respectively. Figure *5.4*(b) and (c) represents the dc bus voltage behavior and ac side frequency fluctuations under injected perturbations. The dc bus voltage and ac system frequency remain intact to their reference values. The novel IDO applied in the microgrid system, that reduces the event counts subjected to noise added as shown in Figure *5.5*(a). whereas if the IDO is not implemented the controller event counts are enhanced as shown in Figure *5.5*(b).

The ETC automatically executed when the system trajectory crosses the inequality (*5.20*). The results shown in Figure *5.5* verifies the event trigger strategy for resource utilization as the control effort remains constant in between two consecutives inter execution times T_{ie}. In Figure *5.6* the error sliding surfaces are shown converging to their equilibrium point.

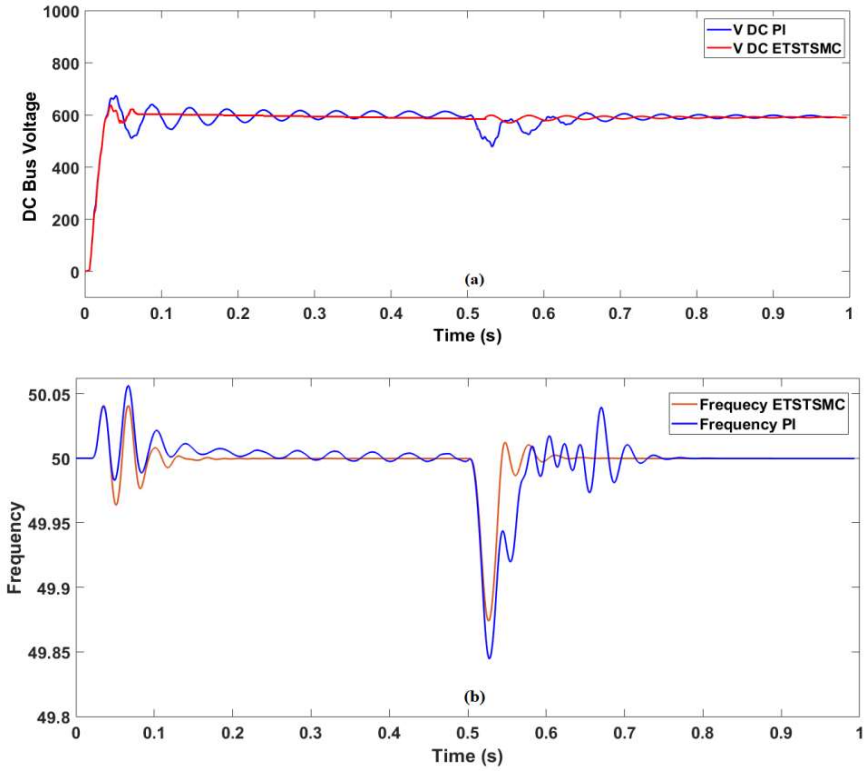

Figure 5.7. PI and ETSTSMC comparison (a) DC bus voltage response (b) Inverter side frequency response.

Also the superior performance of ETSTSMC scheme is achieved when it is compared with PI control with current control transfer gain $I_{gain}(s) = \left(1.5 + \frac{18.32}{s}\right)$ and amplitude control transfer gain $G_{gain}(s) = \left(0.92 + \frac{648.4}{s}\right)$ under the grid connected and islanded mode operation as shown in Figure *5.7*. Here the perturbation is introduced by disconnecting microgrid from utility grid after 0.5s. Triggering instants where the control efforts are updated are shown in Figure *5.8*. Control performance of finite time ETSTSMC control algorithm proposed in the chapter of the thesis, control technique with SMC having power rate reaching law [117] (as explained in section 5.3) and Nonlinear disturbance observer (NDO) based controller explained in [96] are applied on the system depicted in Figure *5.1* as per specifications provided in Table *5.1*. Response of these control actions are on DC bus voltage is shown in Figure *5.9*. Super twisting reaching law (*5.17*) consist of additional integral surface term S_2 which gives the fast-reaching response along with chattering suppression as compared to PRSMC [117]. NDO being implemented in the chapter of the thesis exhibits distortion in the steady state. On the other hand, due to

the incorporation of integral phenomena in context of designing the disturbance observer steady state response is significantly improved. The comparative assessment of response is reflected in Figure *5.9*.

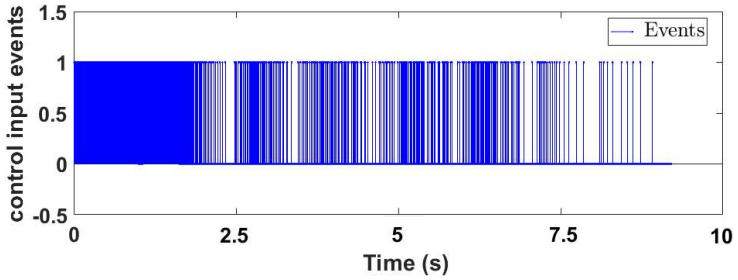

Figure 5.8. Triggering control events.

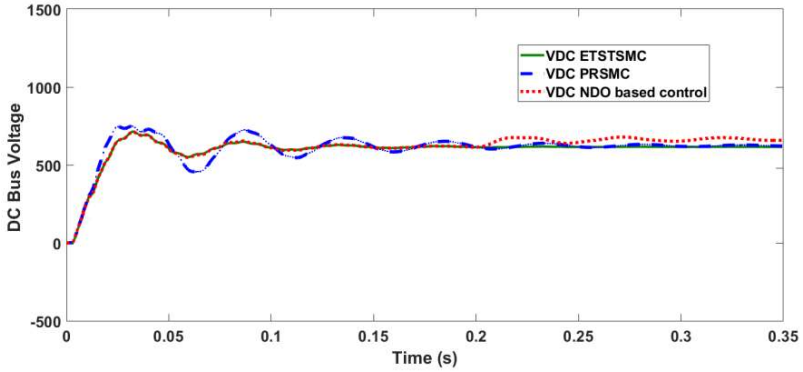

Figure 5.9. DC bus voltage response under ETSTSMC, RTSMC & NDO based control.

5.5.1. Typhoon based real time simulation results verification.

The ETSTSMC is tested in real time simulator Typhoon, Typhoon setup is depicted in Figure *5.10*. Typhoon HIL is a Real-time simulation tool where in Control Centre software microgrid model is developed and Simulation is performed. The results are verified in Real-time using Typhoon HIL 402 Real-time simulator. Typhoon HIL 402 has Xilinx Zynq 7 SoC as main processor and 1 ARM and 1 micro-blaze as secondary processor with 32 Analog I/O and 64 Digital I/O. After testing in real-time, codes are generated from Typhoon HIL in CCS and dumped on TI F28335 DSP card using C2000 DSP interface board. In this way Controller Hardware-in-the-Loop Simulation is performed, and control performance is validated in three platforms i.e. simulation, real-time simulation, and Controller Hardware-in-the-Loop Simulation.

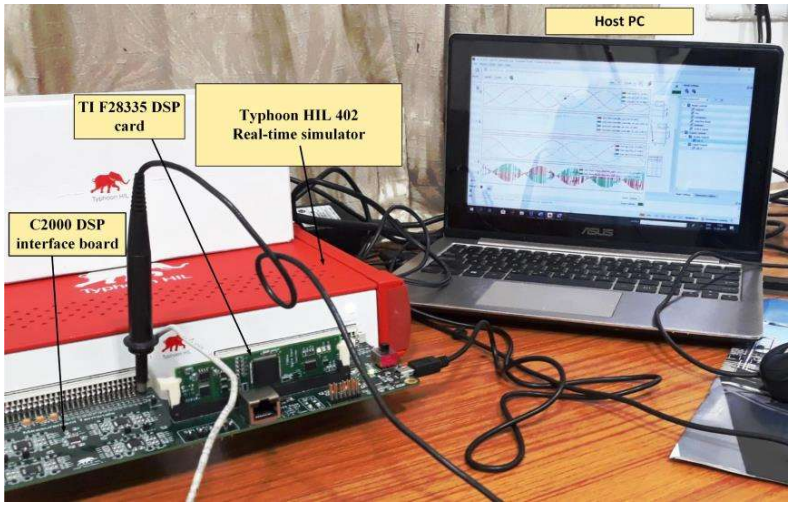

Figure 5.10. Typhoon based CHIL.

The dc bus voltage transition is tested under Power rate reaching SMC and ETSTSMC controller subjected to the grid connection and disconnection and shown in Figure *5.11*(a) and (b) respectively. The ETSTSMC controller transitions are compensated with fast response and least overshoot as depicted in Figure *5.12*.

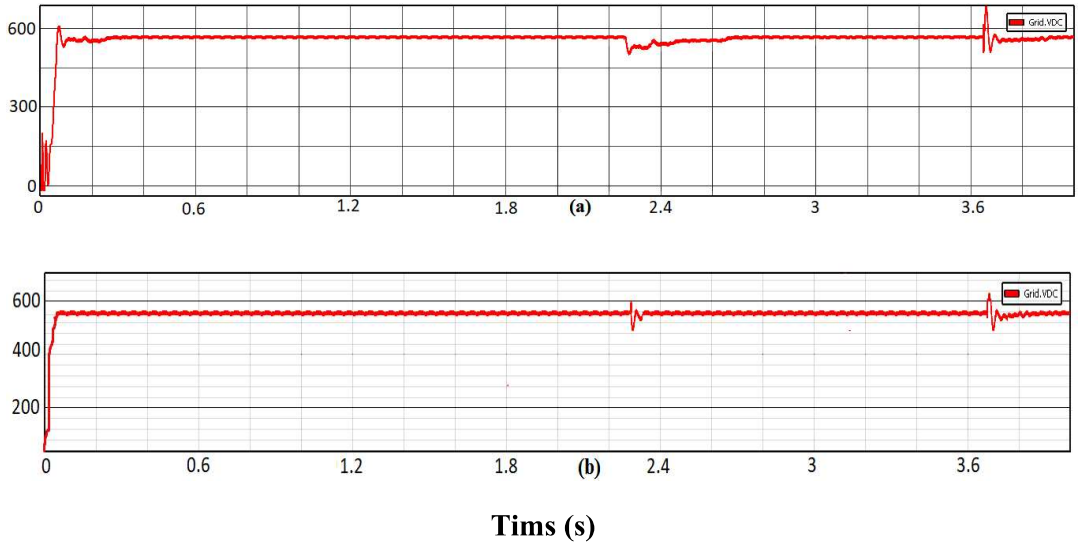

Figure 5.11. DC bus voltage response in Typhoon CHIL (a) PRSMC-response (b) ETSTSMC response.

The equivalent control inputs U_{eq1} *and* U_{eq2} variation in real time environment is shown in Figure *5.12*(a) and (b). Here it is verified that the control inputs remain constant between two consecutives inter execution times and thus extra control efforts can be presides. enlarge view of ETC is indicated in circle shown in Figure *5.12*(b). Frequency transient responses for ETSTSMC (F2) and Power rate reaching SMC (PRSMC) (F1) controller in

typhoon is shown in Figure *5.13*. Figure *5.14* shows the dc bus regulation under grid connected to islanded and vice-versa transitions. The Figure *5.14*(a) shows 3-Ø voltage output of inverter, Figure *5.14*(b) shows the inverter current and Figure *5.14*(c) depicts the dc bus voltage. DC bus voltage fluctuation band under ETSTSMC controller is indicated by circle in Figure *5.14*(c). Performance of the controller is tested for unbalance load in real time by Typhoon based CHIL in Figure *5.15*.

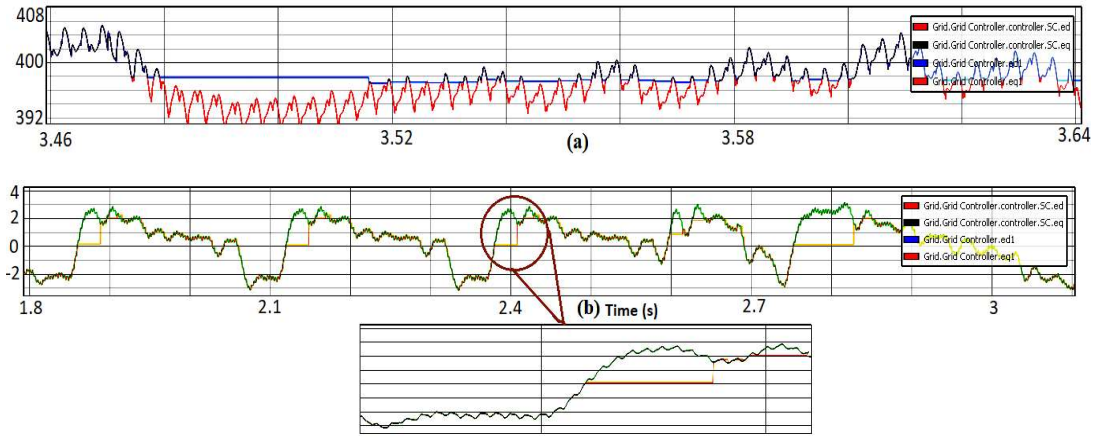

Figure 5.12. ETSTSMC action in CHIL (a) U_{eq1} (b) U_{eq2}.

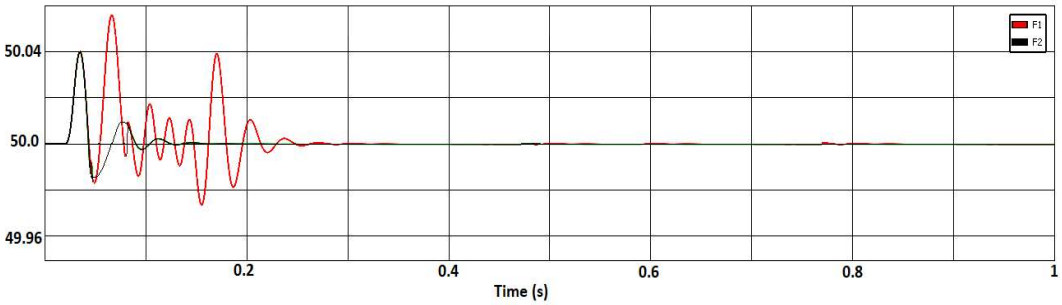

Figure 5.13. Inverter side frequency response of PRSMC controller and ETSTSMC controller in CHIL.

As shown in Figure *5.15* the unbalance load is connected at 2.8s, the inverter currents become unbalance, but the inverter reference modulation voltage magnitude remained constant and maintains the desired voltage level under unbalance load condition. Unbalance load is created by connecting different RL loads to each phase. ETSTSMC has achieved fast convergent & reduce overshoot response validates the proposed technique.

5.5.2. Result Discussion and Main findings.

Results obtained in Figure *5.4* verifies the robust behavior of the controller under disturbances. Figure *5.5* depicts the result obtained by triggering of control events and

reduced event count under IDO operation. In Figure *5.6* the fast and finite time convergence of the error states fact is verified. The noise reduction capability of IDO is justified through the result shown in Figure *5.7* & Figure *5.9* represents the improved transient and steady state performance of the controller whereas Figure *5.8* shows the triggering time of events. All results obtained through Typhoon HIL 402 Real-time simulator in the CHIL platform are again verified the controller objectives as shown in Figure *5.11* to Figure *5.15* respectively. These results obtained confirm that the chattering free ETSTSMC control achieves the objective of optimized control triggering, robust performance, and improved finite time response under various system uncertainties.

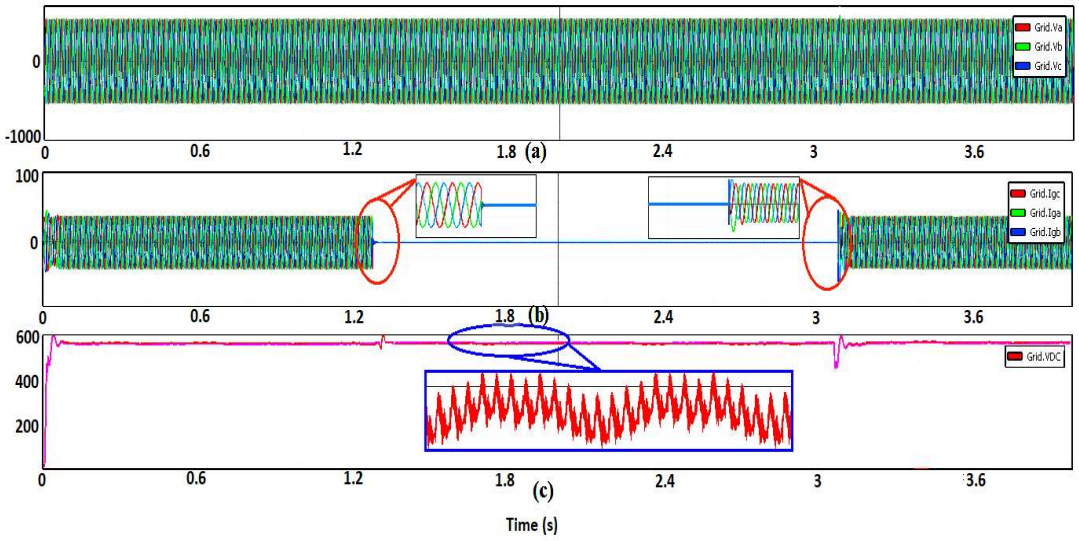

Figure 5.14. No load disturbance (a) Inverter output Voltage (b) Inverter Current (d) DC bus Voltage.

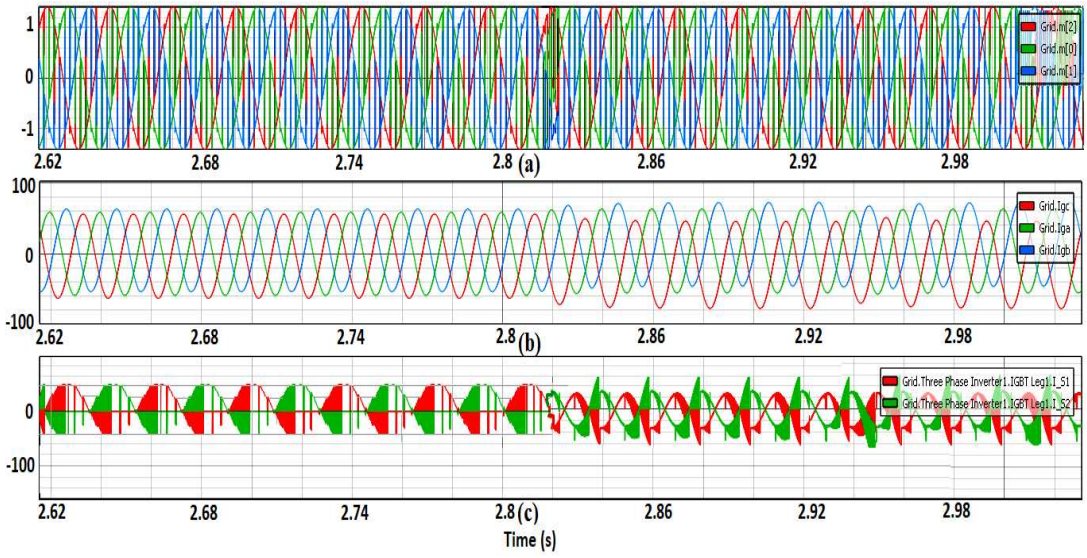

Figure 5.15. Unbalance load disturbance (a) Inverter reference modulation wave (b) Output current (c) Inverter switch currents.

5.6 Summary

An approach to compensate both matched/unmatched uncertainties in a microgrid through novel IDO is proved. IDO is based on SMC technique with super twisting reaching law. The event control triggering is applied to optimize control efforts in addition to super twisting SMC. Firstly, the robust SMC is applied for disturbance rejection then the triggering of control is applied at condition followed by the execution instant. Microgrid system states are stabilized in finite time under various disturbances simultaneously through the proposed controller. The efficacy of the proposed controller is more than that of other control law is verifies with various lemmas. As a matter of fact, all the results demonstrated the robust behavior of the proposed controller both in simulation as well as CHIL platform.